Selective Conversion of Glucose to 5-Hydroxymethylfurfural by Using L-Type Zeolites with Different Morphologies

María José Ginés-Molina, Nur Hidayahni Ahmad, Sandra Mérida-Morales, Cristina García-Sancho, Svetlana Mintova, Eng-Poh Ng, Pedro Maireles-Torres

HAL Id: hal-02893855
https://hal.science/hal-02893855

Selective conversion of glucose to 5-hydroxymethylfurfural by using L-type zeolites with different morphologies

María José Ginés-Molina,[a,*] Nur Hidayahni Ahmad,[b,*] Sandra Mérida-Morales,[a,*] Cristina García-Sancho[a,*], Svetlana Mintova,[c] Eng-Poh Ng[b,**] Pedro Maireles-Torres[a,**]

[a] Departamento de Química Inorgánica Cristalografía y Mineralogía (Unidad Asociada al ICP-CSIC) Facultad de Ciencias Campus de Teatinos, Universidad de Málaga, 29071 Málaga, Spain.

[b] School of Chemical Sciences, Universiti Sains Malaysia, 11800 USM, Penang, Malaysia.

[c] Laboratoire Catalyse & Spectrochimie, ENSICAEN, Université de Caen, 14000 Caen, France.

[*]These authors contributed equally to this work as first author.

[**]Corresponding authors. E-mail address: maireles@uma.es (PMT); epng@usm.my (EPN)

Abstract

The catalytic dehydration of glucose to 5-hydroxymethuylfurfural (HMF) requires the development of selective solid acid catalysts, bearing different types of acid-base active sites. In the present work, the morphology of an L-type zeolite (LTL topology) has been modified in order to evaluate the influence of several protonated-form LTL zeolites with different morphologies on their stability and catalytic performance in glucose conversion to 5-HMF. Physico-chemical characterisation of LTL-based catalysts has revealed that the three types of morphologies (needle, short rod and cylinder) are active, with complete glucose conversion and high HMF yield values. The addition of $CaCl_2$ had a positive influence on the catalytic performance, improving the partition coefficient in the biphasic water:methyl isobutyl ketone system for efficiently extracting HMF formed from the aqueous phase. It was found that

morphology influences the textural and acid properties of LTL zeolites, and hence their catalytic performance. The best catalytic results have been obtained with the NEEDLE-LTL, showing nanoparticles with a length of 4.03 nm and a width of 0.63 nm, which attains a HMF yield of 63.1%, at 175 ℃ after 90 min of reaction, and a glucose conversion of 87.9%. The reusability study has revealed a progressive decrease in HMF yield after each catalytic cycle. Different regeneration methods have been essayed (washing with solvents and calcination), without recovering the initial catalytic activity. The presence of organic molecules in the micropores has been demonstrated by TG-DTA analysis, which are difficult to remove even after a regeneration process at 550 ℃.

Keywords: *biomass; glucose; 5-hydroxymethylfurfural; LTL zeolite; heterogeneous catalysis*

1.   Introduction

In recent years, much attention is being paid to the development of environmentally and economically viable synthetic routes and technologies for producing chemicals and fuels from non-fossil carbon sources as alternative to fossil raw materials [1]. In this context, biomass is emerging as a very promising sustainable feedstock, being the only widely available and renewable carbon source [2,3]. Lignocellulosic biomass, mainly composed by lignin, cellulose and hemicellulose, with an estimated annual production about 2×10^{11} metric tons, is the most abundant source of carbohydrates, but physico-chemical treatments are required for its use as a raw material [4]. Although lignocellulose is a sustainable resource for production of biofuels and chemicals, it is necessary that this does not interfere with the food chain. The hydrolysis of cellulose and hemicellulose leads to monomeric C5 and C6 sugars, which can be converted into important platform molecules, such as furfural and 5-hydroxymethylfurfural (HMF), respectively, which are the starting point for the synthesis of a large variety of biofuels and chemicals [5,6]. For instance, HMF can be transformed into 2,5-dimethylfuran [7] or

2

levulinic acid [8,9], among others, which are key intermediates for the synthesis of pharmaceuticals, polymers or biofuels.

Although the dehydration of fructose to HMF has largely been reported in the literature, glucose is preferred due to its abundance and low price [10]. There is not a general consensus about the mechanism of glucose dehydration to HMF, even though a generally accepted route based on: (i) isomerization of glucose to fructose, and (ii) dehydration of fructose to HMF [4]. The first step is considerably difficult and requires Lewis acid or basic sites, being the limiting factor for HMF production. The reaction may be performed either in water, organic solvents or ionic liquids, in particular polar aprotic solvents. Homogeneous catalysts such as sulphuric or hydrochloric acids can be effective for the hydrolysis of cellulose to glucose, and even for the dehydration of fructose to HMF. However, due to their corrosive properties which are hazardous for equipment, so they are gradually replaced by heterogeneous catalysts. Besides, heterogeneous catalysts allow their easy separation from solution, recovery and reuse [11–13]. Different solid acid catalysts have been tested for dehydration of glucose to HMF, such as γ-Al_2O_3 [14], zeolites [15], metal oxides like TiO_2 or ZrO_2 [12-15], mesoporous solids [16,17] inter alia.

Nevertheless, both solvent and catalyst must be considered as two key factors to attain high HMF yields from C6 carbohydrates. A common strategy is the use of biphasic systems for furfural production, because this approach allows higher HMF yields than those systems employing only water. Usually, the biphasic medium is formed by the addition of organic solvents (toluene, methyl isobutyl ketone, among other) to an aqueous solution, or the addition of miscible organic solvents like tetrahydrofuran (THF) [18], to a saturated salt solution, which allows to extract the HMF formed from the aqueous phase, preventing its further degradation and condensation [4].

In order to prevent these side reactions, Román-Leshkov *et al.* [19] employed inorganic salts in a biphasic system for dehydration of fructose to HMF and concluded that the salting-out effect leading to a higher partition coefficient, limiting the individual cationic or anionic contributions, so then it is feasible to correlate to the interaction of all ionic species. In this context, it has also been reported that divalent cations interact more strongly with saccharides than the monovalent ones [20]. Thus, Combs *et al.* [21] observed that alkaline earth metal cations can form bidentate complexes with glucose, which accelerated its transformation. Later, our research group studied the beneficial effects of $CaCl_2$ on glucose dehydration to HMF in the presence of Al_2O_3 as catalyst, in such a way that the addition of $CaCl_2$ to the reaction medium notably improved the catalytic performance, even at very short reaction times, due to the interaction between Ca^{2+} ions and glucose molecules, which favored the α-D-glucopyranose formation [14].

Concerning the use of zeolites for glucose dehydration, different acidic ZSM-5 zeolites (H-, Fe- and Cu-ZSM-5) were prepared and studied by modifying several experimental variables [15]. It was demonstrated the positive effect of the addition of inorganic salt (NaCl) to a biphasic (water/MIBK) system, since a glucose conversion of 80%, with a HMF yield of 42% was attained at 195 °C, after 30 min, by using a H-ZSM-5 zeolite, which had the lowest Lewis/Brönsted ratio among the studied zeolites. Later, the H-ZSM-5 zeolite was compared with H-Y and H-Beta zeolites, in order to assess the influence of the textural properties on the catalytic performance in glucose dehydration [22]. Under similar experimental conditions, by using a H-Beta, the highest HMF yield (56%) was reached, thus demonstrating the benefit of mesoporosity in this catalytic process.

Recently, by using a bifunctional Cr/β zeolite, a high selectivity to HMF with a yield of 72%, was found at 150 °C, after 90 min, by adding NaCl to a biphasic H_2O/THF system [23].

After three consecutive catalytic cycles, the catalytic activity slightly decreased, but after a thermal treatment was almost recovered.

Morphological or textural characteristics play a highly important role when discussing catalytic activity in a chemical reaction [Y.J. Huang, G.R. Qi, L.S. Chen, Appl. Catal. A: Gen. 240 (2003) 263-271]. Nevertheless, the morphological roles of zeolite in glucose dehydration are still not completely understood and hence further investigation to reveal this effect in this reaction is utmost important. The aim of this work is a thorough study of glucose dehydration for HMF production using protonated L-type (H-LTL) zeolites with different morphologies, which have been characterized and their catalytic performance has been correlated with their textural and acid-base properties.

2.   Results and Discussion

2.1.   Catalyst Characterization

The choice of an LTL zeolitic framework to evaluate the influence of the morphology (short rod, cylinder and needle) on the catalytic performance in glucose dehydration to HMF arises from the dimensions of pore mouth and channels of this crystallographic structure (**Figure 1**). These allow the entrance of glucose molecules to reach active acid sites, and 5-hydroxymethylfurfural can easily go out, leaving active sites available for new sugar molecules.
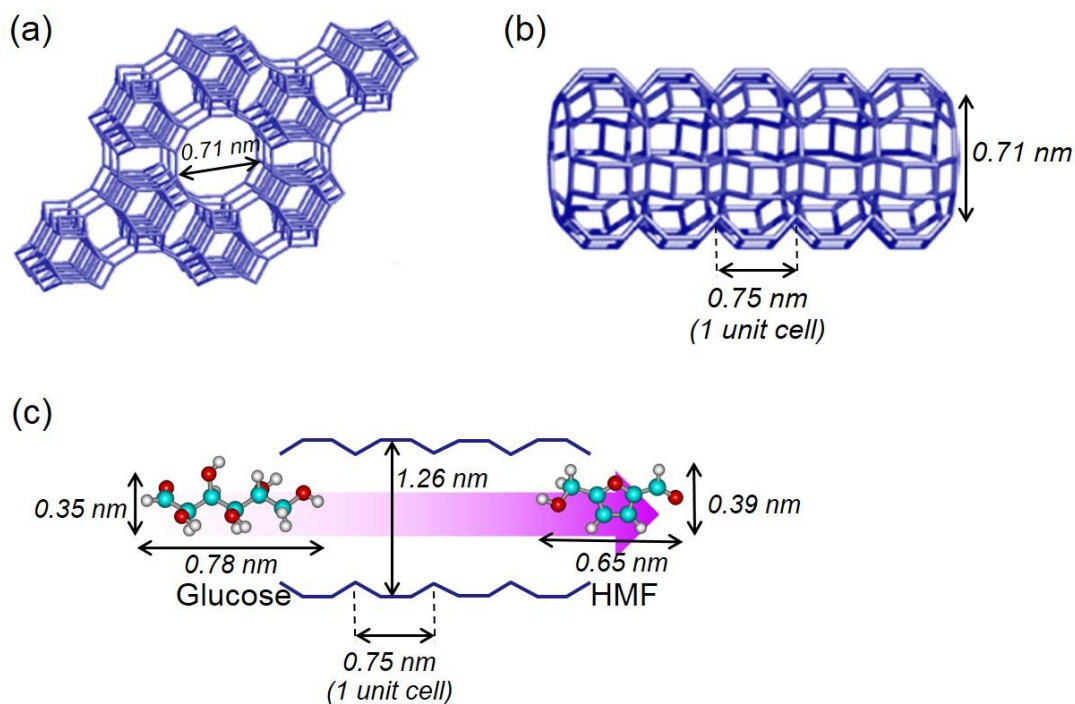
Figure 1. (a) Structure of zeolite LTL view along [001] plane illustrating its hexagonal framework. (b) An LTL channel view normal to [001] plane that consists of 0.71 nm unit cells with a pore opening of 0.71 nm. (c) Schematic illustration of diffusion of glucose as reactant and HMF as product in the 12-membered ring channel of LTL zeolite.

The X-ray diffraction patterns of H-LTL zeolites exhibit many narrow diffraction peaks at $2\theta = $ XXX° (100), XXX° (200), XXX° (001), XXX° (210), XXX° (111), XXX° (220), XXX° (310), XXX° (301), etc. which can be assigned to the hexagonal LTL-type framework (PDF 98-007-4170) (**Figure 2**). In all cases, neither additional crystalline phase nor amorphization is detected and the crystallinity of the solids is preserved after ion-exchange and calcination treatments.
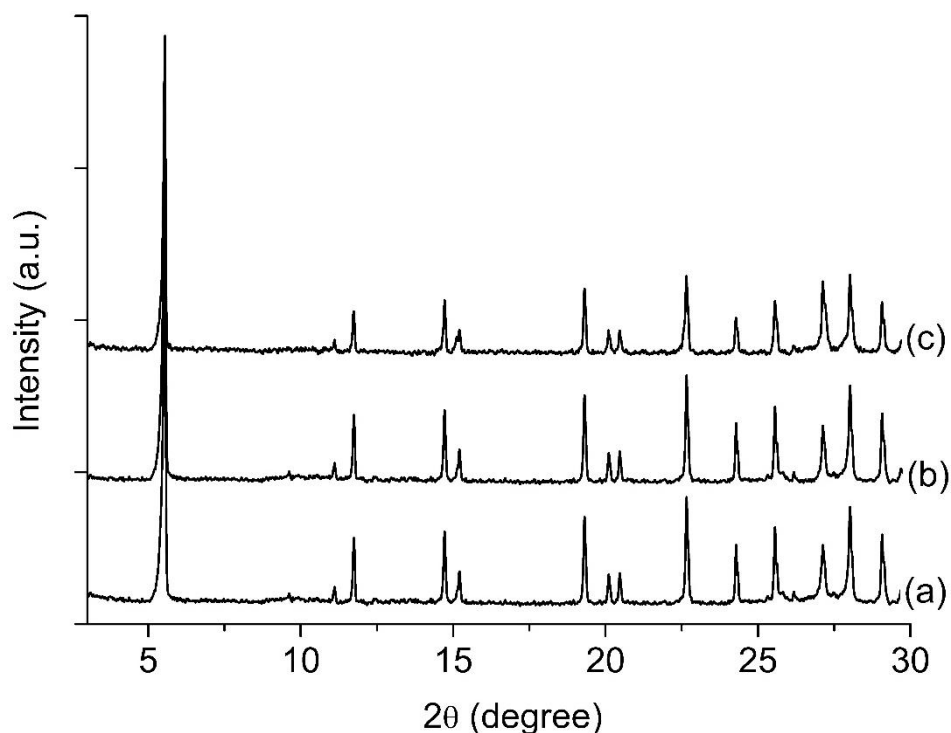
Figure 2. XRD patterns of (a) ROD-LTL, (b) NEEDLE-LTL and (c) CYL-LTL zeolites.

Concerning the chemical composition of LTL zeolites, the Si/Al molar ratio values obtained from ICP-OES are close to 3, which are lower than that used in the synthesis gel (10) (**Table 1**). The comparison between the bulk and surface chemical composition data, deduced from ICP-OES and XPS, respectively, points an enrichment of Si on the surface of LTL-zeolites. This could be explained by the higher Si/Al molar ratio (10) used in the synthesis of these zeolites. However, it must be taken into account the inherent error associated to the semi-quantitative analysis by XPS. After the ion exchange process between K^+ and NH_4^+ ions, not all the alkaline cations are removed, which can be due to the existence of strong acid sites remaining dissociated and neutralized by K^+ cations, even in the presence of an excessive ammonium solution. Therefore, the K/Al molar ratio is lower than 1 for NEEDLE-LTL and ROD-LTL, indicating that, although acid sites are protonated, a fraction of sites is still occupied

by K^+ ions. This fraction is even higher for the CYL-LTL, where the value is closed to 1 would point out that this morphology is the less favorable for the ion-exchange process.

Table 1. XPS and ICP-OES (* in parentheses) data of LTL zeolites, as determined from XPS analysis.

Samples	Binding energy (eV)				Si/Al molar ratio*	K/Al molar ratio*
	Si 2p	Al 2p	O 1s	K $2p_{3/2}$		
NEEDLE-LTL	102.8	74.3	532.1	293.3	4.23 (3.00)	0.45 (0.63)
ROD-LTL	102.9	74.5	532.2	293.4	4.54 (2.90)	0.45 (0.55)
CYL-LTL	103.2	74.6	532.4	293.7	4.43 (3.45)	1.28 (1.07)

X-ray photoelectron spectroscopy (XPS) has been used to get insights into the surface nature of LTL-based zeolites. In all cases, the binding energies of Si 2p (102.8-103.2 eV), Al 2p (74.3-74.6 eV) and O 1s (532.1-532.4 eV) are typical of these elements forming part of microporous aluminosilicates [24]. As regards the K 2p spectra, they exhibit the typical doublet with the K $2p_{3/2}$ at 293.3-293.7 eV, and a spectral separation of 2.8 eV, typical of K^+ ions [25].

On the other hand, textural properties reveal that all zeolites maintain high surface area values, being the largest one for short rod morphology (**Table 2**). As expected, these zeolites are mainly microporous solids, with a percentage of microporous surface area higher than 95%.

Table 2. Textural and acid properties of LTL zeolites

| | $S_{Langmuir}$ | S_{micro} | V_p | Length | Width | Total acidity |
	$(m^2\ g^{-1})$	$(m^2\ g^{-1})$	$(cm^3\ g^{-1})$	(μm)	(μm)	$(\mu mol\ m^{-2})^*$
NEEDLE-LTL	248	235	0.100	4.03	0.63	6.73
ROD-LTL	303	293	0.120	1.39	1.38	6.17
CYL-LTL	219	199	0.090	2.18	0.97	4.88

*Determined from NH_3-TPD

The microporous nature of these LTL-based zeolites can be easily confirmed by the shape of their adsorption-desorption isotherms of N_2 at -196 ºC, which are Type I in the IUPAC classification, typical of microporous solids (**Figure 4**). The slight hysteresis loop could be associated to some mesoporosities generated during treatments used for synthesizing their protonated forms, probably associated to interparticular voids [26,27], which is corroborated by the pore size distribution curves (Figure 4, bottom).
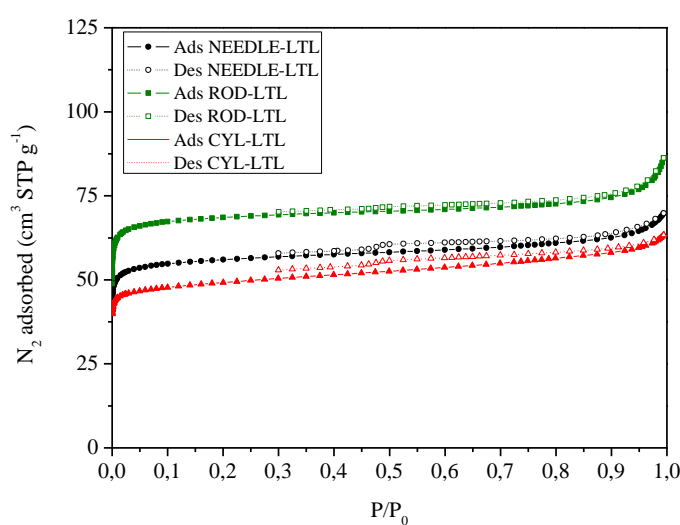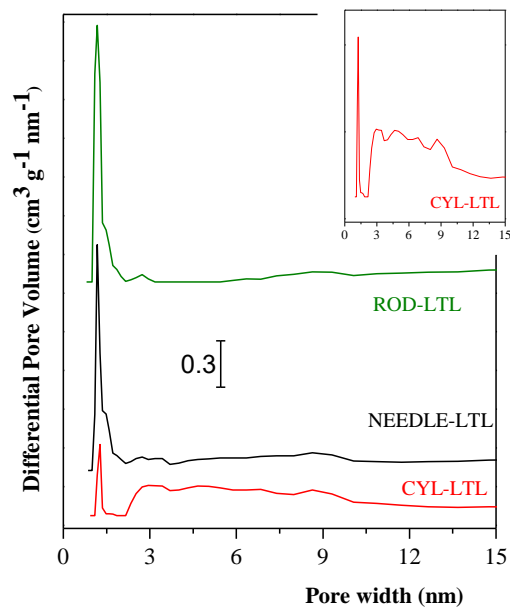
Figure 4. N$_2$ adsorption-desorption isotherms (top) and pore size distributions (bottom) of

LTL zeolites at -196 ºC.

The different morphologies are more clearly appreciated in the scanning electron micrographs (**Figure 5**), where micrometric particles are observed, whose dimensions and shapes fit in really well with short rods, needles and cylinders (**Table 2**).
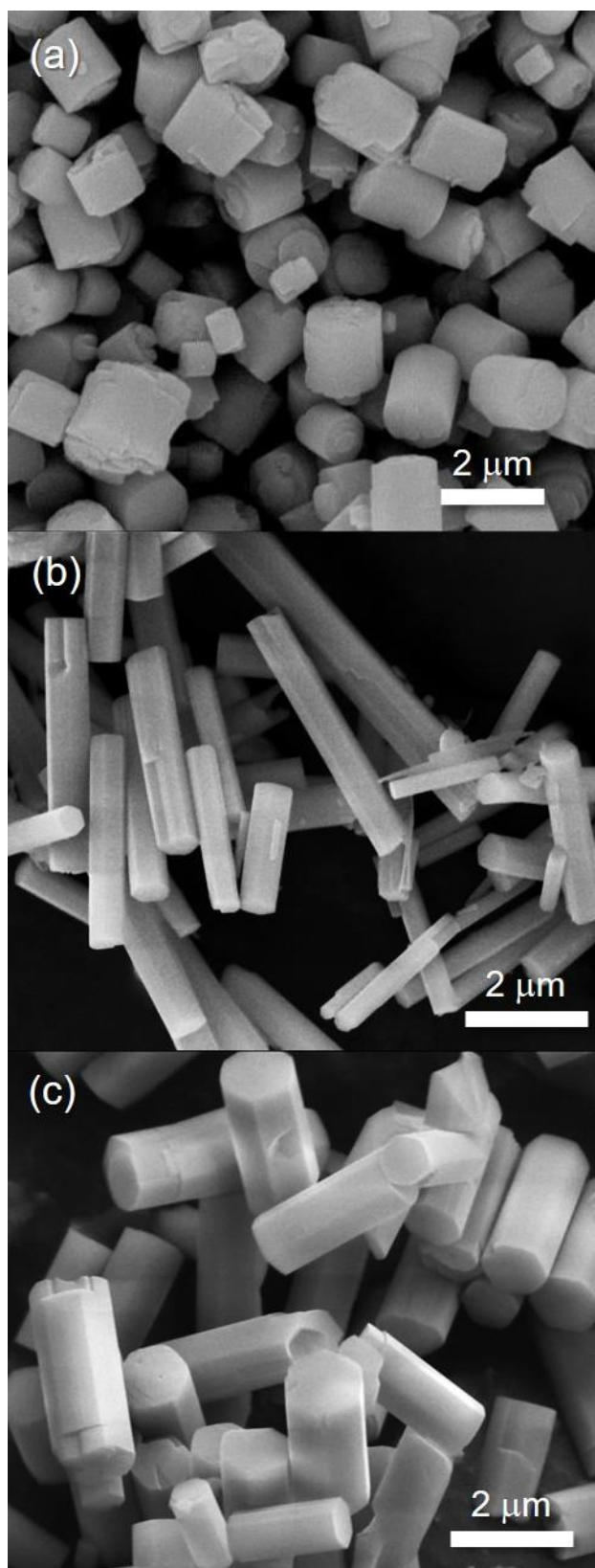
Figure 5. SEM images of zeolite LTL crystals synthesized of (a) ROD-LTL, (b) NEEDLE-

LTL and (c) CYL-LTL. Scale bar = 2 µm.

On the other hand, the chemical environment of aluminium has been analysed by ^{27}Al MAS-NMR spectroscopy (**Figure 6**). Extra-framework octahedral Al species are associated to a resonance signal at a chemical shift near 0 ppm, whereas tetrahedral Al in crystallographic sites in the zeolite framework appears at about 60 ppm. This latter signal is observed in all cases, and the absence of broadening effect at lower chemical shift values could discard the existence of pentacoordinated or distorted tetrahedral aluminium, reported in other microporous aluminosilicates, which give rise to signals at 30 and 47 ppm, respectively [28–30]. The small contribution at 0 ppm is associated to extra-framework Al species, but this is absent in the MAS-NMR spectrum of CYL-LTL, where all Al seems to be in tetrahedral coordination.
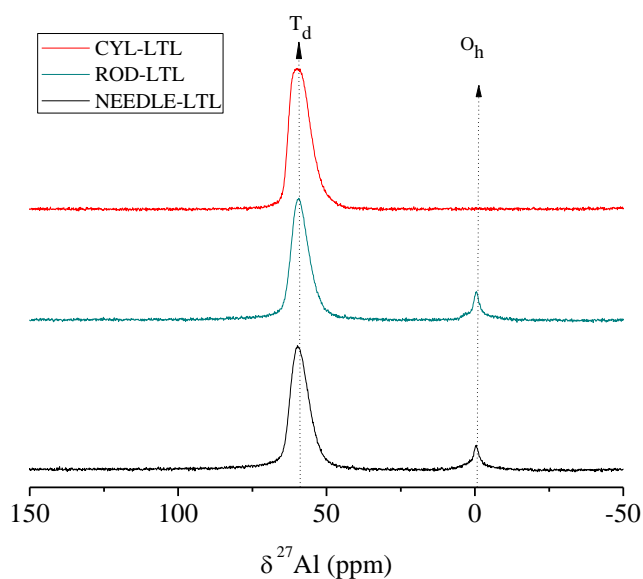
Figure 6. [27]Al Solid State Nuclear Magnetic Resonance spectra of LTL zeolites.

The total acidity of catalysts was determined from ammonia temperature-programmed desorption (NH$_3$-TPD), whereas the nature (Brönsted or Lewis) of acid sites was studied from pyridine adsorption coupled to FTIR spectroscopy. **Figure 7** displays the amount of ammonia desorbed in different temperature ranges, which have been assigned to weak (100-200 ºC), medium (200-300 ºC) and strong (300-550 ºC) acid sites. The total acidity follows the order:

ROD-LTL (1874 µmol g^{-1}) > NEEDLE-LTL (1672 µmol g^{-1}) > CYL-LTL (1065 µmol g^{-1}), being strong acid sites predominant in all cases. This acidity order is the same found for Langmuir surface area values (Table 2).
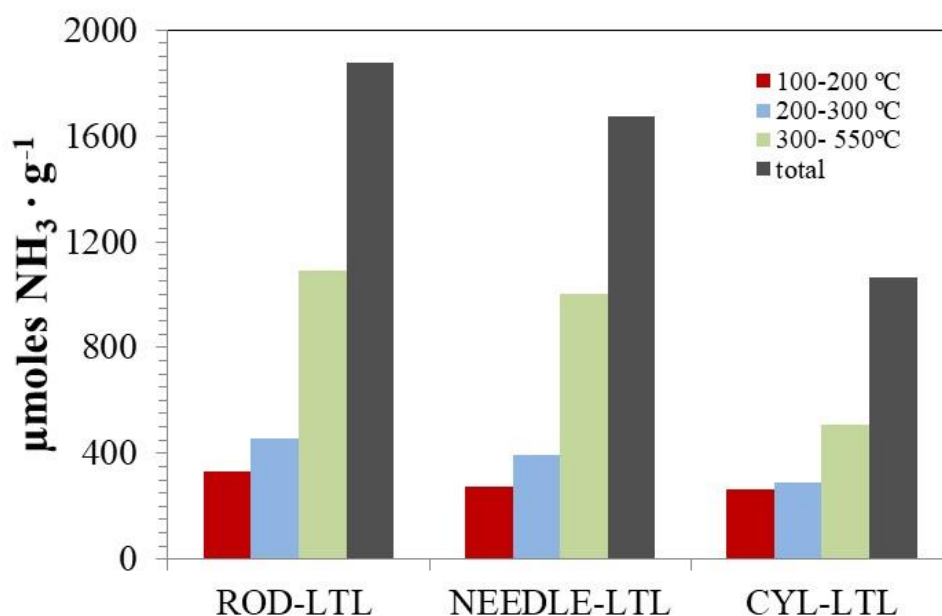
Figure 7. NH$_3$ desorption of LTL-based zeolites, as a function of the strength: weak (100-200 ℃), medium (200-300 ℃) and strong (300-550 ℃).

The nature of acid sites (Brönsted and/or Lewis) has been studied by pyridine adsorption coupled to FTIR spectroscopy. The FTIR spectra after adsorption and subsequent desorption of pyridine at 150 and 300 ℃ are displayed in **Figure 8**, whereas the concentration of Lewis and Brönsted acid sites is given in **Table** 3. The lowest concentration of both Lewis and Brönsted acid sites is found for the ROD-LTL zeolite, which after evacuation at 300 ℃ contains the least amount of Lewis acidity. The other two zeolites (CYL- and NEEDLE-LTL) exhibit considerably similar concentrations of strong Brönsted and Lewis acid sites, calculated from pyridine amount remaining on catalysts after evacuation at 300 ℃. Moreover, these two zeolites also possess nearly similar B/L molar ratio (4.76 and 4.86, respectively). It has been

previously reported that Brönsted acid sites could be associated to distorted tetrahedral Al species located in the zeolite framework, whereas distorted pentacoordinated and octahedral Al species have been associated to Lewis acid sites in zeolites [31].
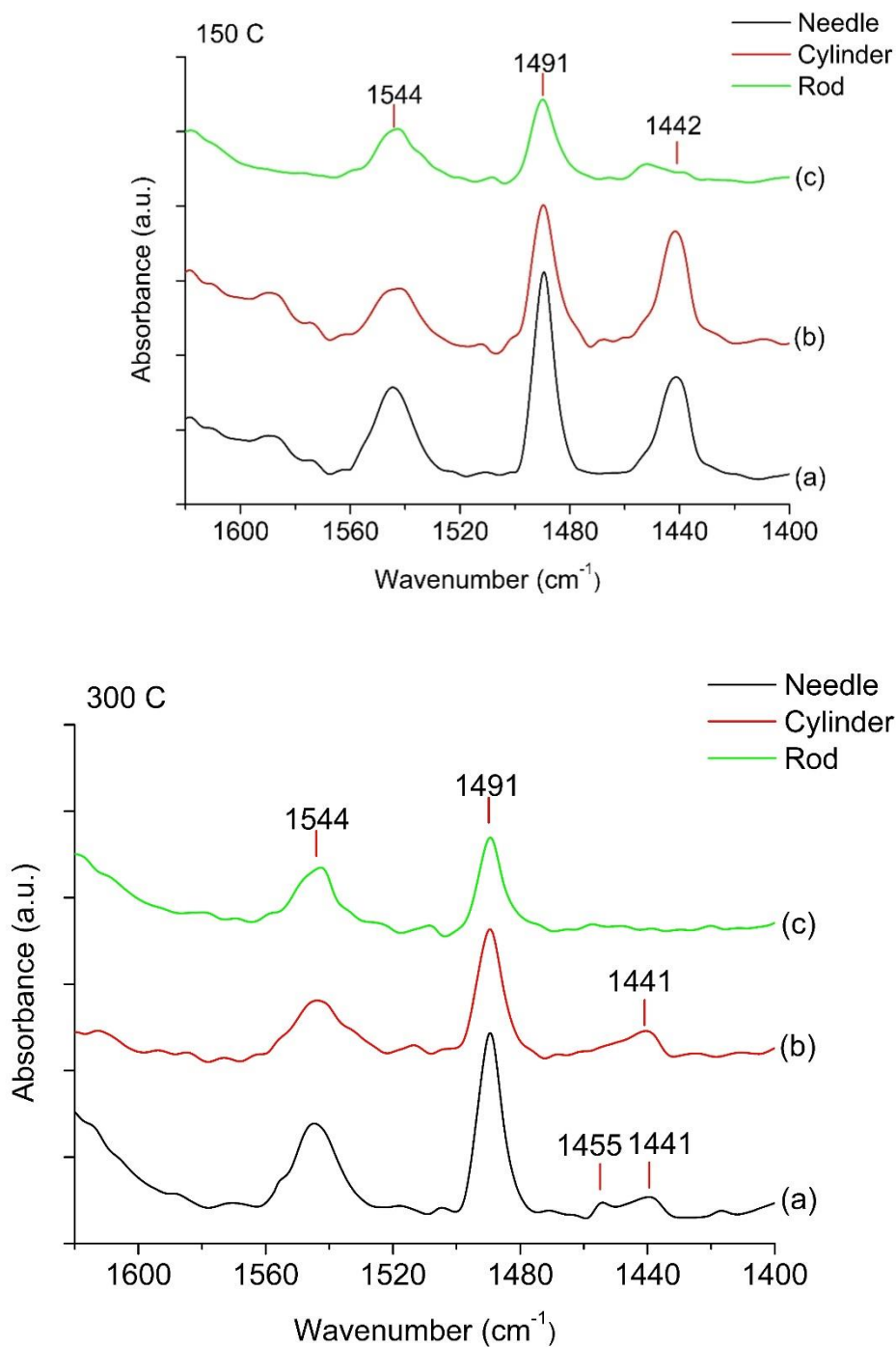
Figure 8. FTIR spectra of LTL zeolites after pyridine desorption at different temperatures (150 and 300 ºC)

Table 3. Surface acidity of zeolite LTL with different morphology at different temperature.

Sample	Py-FTIR Acidity (µmol/g)							
	Lewis (L)		Brönsted (B)		Total (L + B)		B/L	
	150 °C	300 °C	150 °C	300 °C	150 °C	300 °C	150 °C	300 °C
ROD-LTL	33.65	0.00	118.58	84.51	152.23	84.51	3.52	-
CYL-LTL	126.08	32.08	128.07	152.85	254.15	184.93	1.02	4.76
NEEDLE-LTL	120.55	31.76	161.39	154.50	281.95	186.26	1.34	4.86

According to the ^{27}Al NMR data and NH$_3$-TPD, it looks like the pyridine data of CYL and ROD are interchanged.

2.2. Catalytic study

These zeolites have been evaluated as acid catalysts in the dehydration of glucose to 5-hydroxymethylfurfural, an important platform molecule for the synthesis of biofuels and high value-added chemicals. Although the mechanism involved in glucose dehydration to HMF seems to depend on type of catalyst, nature of solvent, among other parameters, it is broadly accepted that the rate-determining step is the isomerization of glucose to fructose [4]. For this reason, most of studies have used fructose as starting sugar. The isomerization process is catalyzed by Lewis acid or basic sites, whereas dehydration of fructose to HMF requires the participation of Brönsted acid sites. The production of HMF from glucose has two main drawbacks associated to the catalytic process, that is, the formation of by-products, such as soluble/insoluble polymers and humins and the rehydration of HMF for giving rise to levulinic and formic acids. These processes decrease the HMF yield and, in some cases, provoke the catalyst deactivation. In this sense, the use of organic co-solvents together with the aqueous

phase containing carbohydrates has been usually reported as a suitable strategy for improving HMF yield. Among these organic solvents, methyl isobutyl ketone is one of most often used due to their benign physico-chemical properties [32]. In this work, a biphasic water-MIBK system was employed to study the dehydration of glucose to HMF.

Moreover, previous studies have demonstrated that the addition of inorganic salts to biphasic phases ameliorates the extraction of 5-HMF from biphasic systems [14,16,19]. In particular, calcium chloride exerts a positive effect on the catalytic performance, even at very short reaction times [14,33]. This was explained by the interaction between Ca^{2+} ions and carbohydrates (glucose and xylose), modifying the corresponding anomeric equilibrium towards the anomer α more prone for the dehydration process, as was concluded from ^{1}H NMR spectroscopy data.

In this sense, the catalytic activity of the LTL-zeolites was studied with and without $CaCl_2$ addition (**Figure 9**). The positive effect is clearly observed, since at 150 ºC, after 60 min of reaction and in the absence of inorganic salt, the conversion of glucose is lower than 20% and in this case the formation of HMF is barely detected (HMF yield < 1%). However, the addition of $CaCl_2$ outstandingly improves the glucose conversion until values higher than 95% for ROD-LTL, with a HMF yield of 58.5%, whereas the rest of catalysts attain conversion and HMF yield values higher than 75% and 25%, respectively. Therefore, these data confirm previous results attained with other families of catalysts in the presence of inorganic salts [15,19].
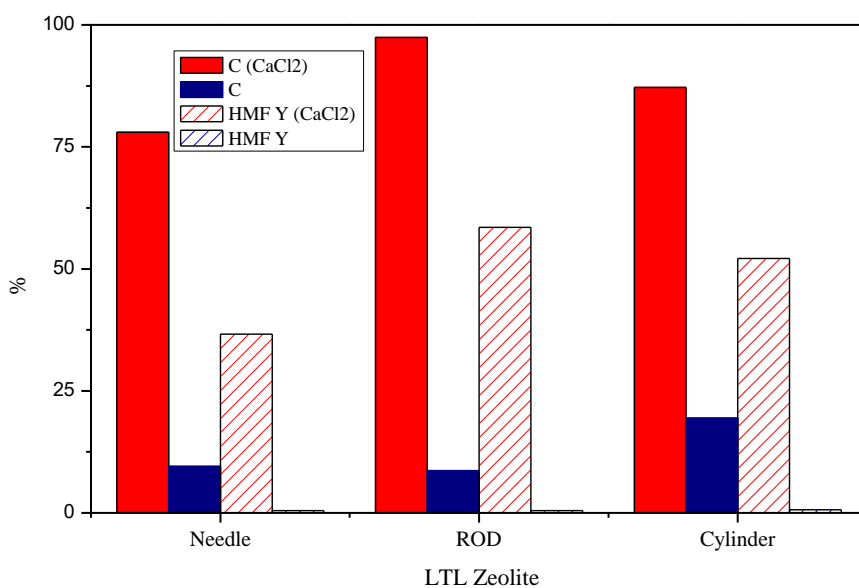
Figure 9. Effect of the addition of $CaCl_2$ on the catalytic performance (Experimental conditions: 0.15 g glucose, 0.05 g catalyst, 1.5 mL water, 3.5 mL MIBK, Temperature= 150 ºC; time = 60 min, $CaCl_2$= 0.65 g $g_{H_2O}^{-1}$).

It is evident the improving effect of $CaCl_2$ addition on the catalytic performance of this series of LTL-based catalysts. However, an additional catalytic study was accomplished in order to evaluate the contribution of $CaCl_2$ to the overall catalytic activity. For this, $CaCl_2$ (0.65 g $g_{H_2O}^{-1}$) was put in contact with glucose in the biphasic system, and compared with the same system to which the NEEDLE-LTL catalyst was added. The data reveal that, in the absence of catalyst, after 3 h at 150 ºC, the glucose conversion was 47.1%, with a HMF yield of 16.8% (**Figure 10**). However, under similar experimental conditions, this catalyst exhibits better catalytic performance, attaining a conversion of 86.9% and a HMF yield of 44.0%. The catalytic activity in the presence of $CaCl_2$ might be explained by the formation of α-anomer in the presence of this salt, as it has been demonstrated in previous studies [14], which could easily be dehydrated due to the thermal contribution (non-catalyzed process) to the overall catalytic performance.
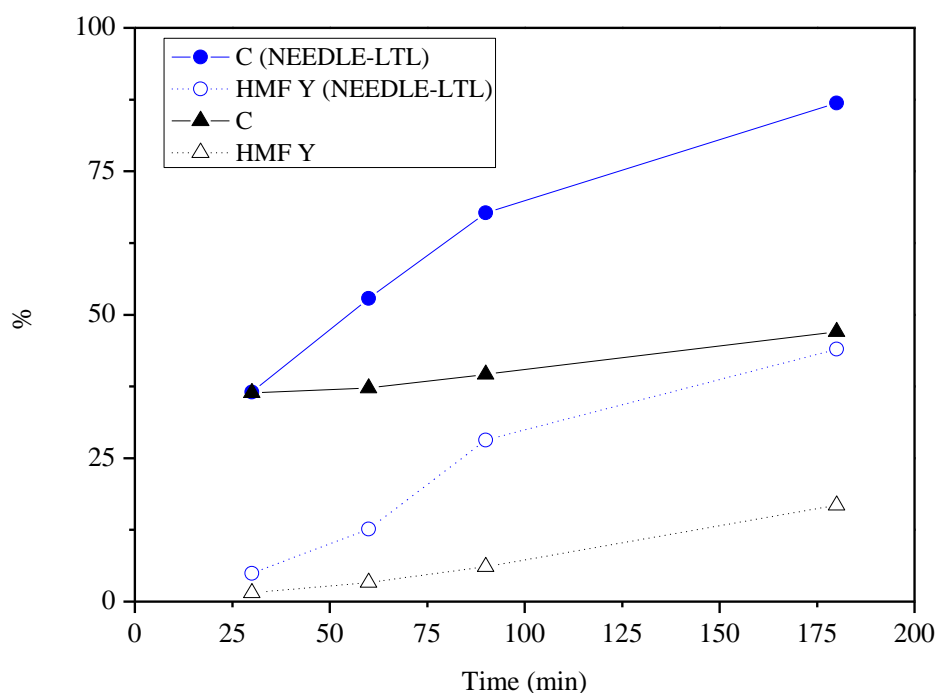
Figure 10. Catalytic performance of $CaCl_2$ and $CaCl_2$/NEEDLE-LTL (Experimental conditions: 0.15 g glucose, straight line: 0.65 g $g_{H_2O}^{-1}$ and 0.05 g NEEDLE-LTL and dash line: 0.65 g $g_{H_2O}^{-1}$, 1.5 mL water, 3.5 mL MIBK, Temperature= 150 ºC)

The kinetics of the dehydration process with LTL-based catalysts were studied at 150 ºC (**Figure 11**), and similar conversion curves were obtained for the three catalysts, in spite of their different acid properties (**Table 2**) and morphologies. However, at intermediate reaction times, the HMF yield values are lower for CYL-LTL, which could be explained by considering its lower acidity, although its mesoporous character could compensate the lower concentration of acid sites in this catalyst. In this study, the highest HMF yield (50.3%) was attained after 300 min with the ROD-LTL catalyst.
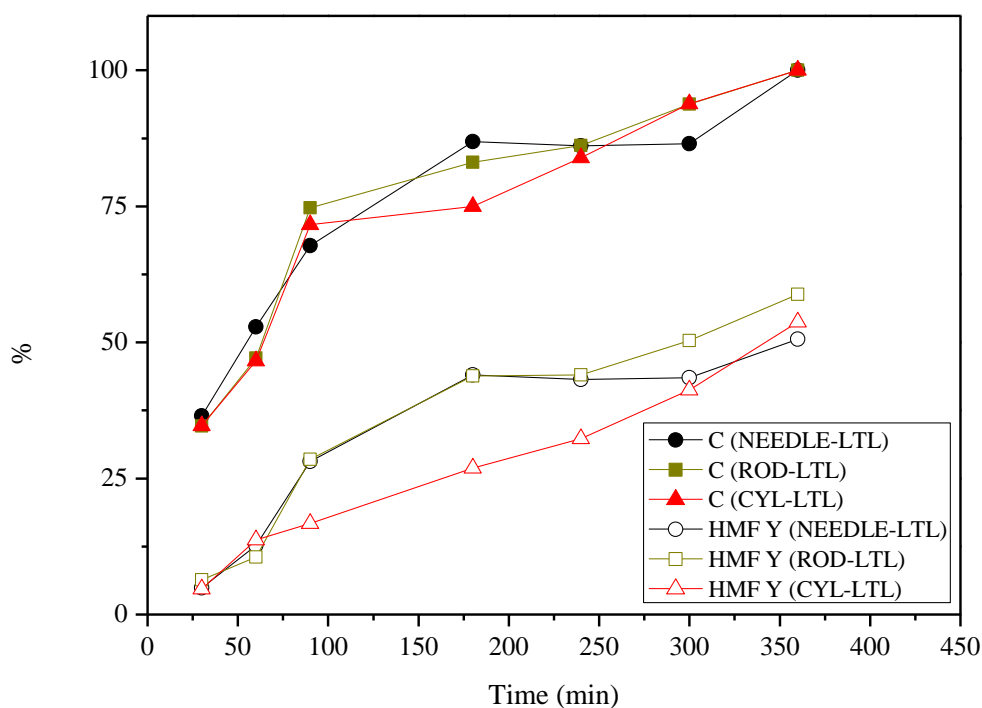
Figure 11. Kinetics of glucose dehydration (Experimental conditions: 0.15 g glucose, 0.05 g catalyst, 1.5 mL water, 3.5 mL MIBK, Temperature= 150 ℃; $CaCl_2$= 0.65 g $g_{H_2O}^{-1}$).

By increasing the temperature until 175 ℃, the reaction time for attaining the highest HMF yield is shortened, being possible to obtain a HMF yield of 63.1% for a glucose conversion of 87.9% with the NEEDLE-LTL catalyst after only 90 min (**Figure 12**). The Figure shows that glucose conversion increases progressively with the reaction time, and values of 100% are already reached after 60 min of reaction time. However, HMF yield values attain a maximum, and then, despite the raise of conversion, degradation processes lead to a decrease in HMF yield.
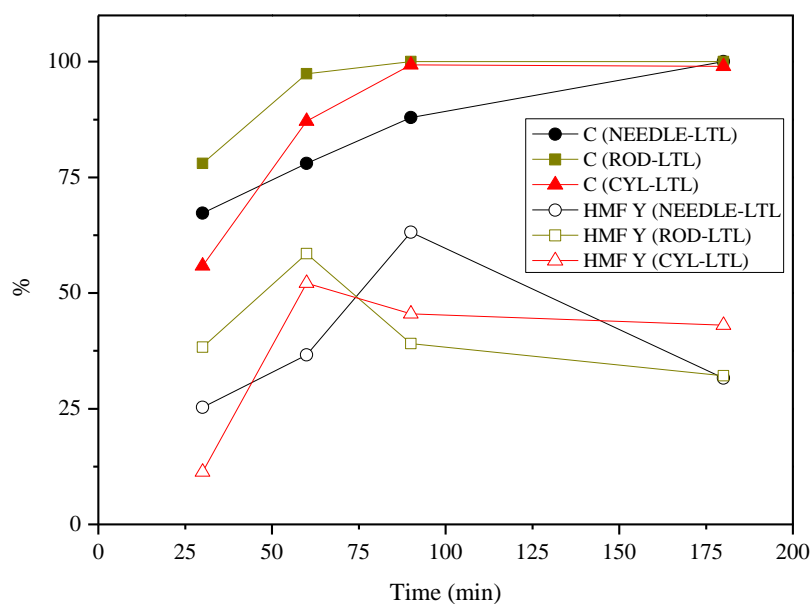
Figure 12. Kinetics of glucose dehydration (Experimental conditions: 0.15 g glucose, 0.05 g catalyst, 1.5 mL water, 3.5 mL MIBK, Temperature= 175 ºC; $CaCl_2$= 0.65 g $g_{H_2O}^{-1}$).

Other experimental parameter evaluated has been the glucose:catalyst weight ratio, which has been varied between 1:1 and 10:1, by maintaining the amount of glucose and adding different amounts of NEEDLE-LTL. It can be observed that conversion of glucose raises with the catalyst loading until a weight ratio of 3:1, which can be explained by the increment of available acid sites for glucose dehydration (**Figure 13**). Nevertheless, a higher amount of catalyst (ratio of 1:1) does not improve the conversion, although a slightly higher HMF yield is attained. This could be explained by considering diffusional problems associated to the location of active sites in micropores.
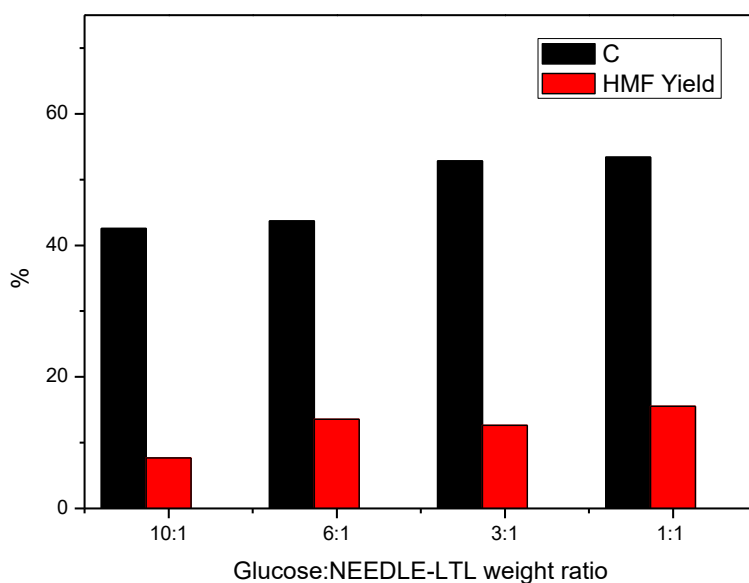
Figure 13. Influence of the glucose:catalyst (NEEDLE-LTL) weight ratio (Experimental

conditions: 0.15 g glucose, 1.5 water, 3.5 mL MIBK, Temperature: 150 ℃; time: 60 min,

$CaCl_2$= 0.65 g $g_{H_2O}^{-1}$).

A key aspect in heterogeneous catalysis is the recovery of the solid catalyst to be used in successive catalytic runs. In order to carry out this study, a glucose:catalyst weight ratio of 1:1 was used, since a higher catalyst loading would minimize the loss of catalyst between cycles, produced by catalyst handling. The reaction was studied at 150 ℃, for 60 min (**Figure 14**). After the first catalytic cycle, the solid catalyst was filtered and dried at 65 ℃. The catalytic data reveal a decrease in glucose conversion from 53.4 to 43.4%, although active sites involved in glucose dehydration to HMF seem to be almost deactivated, since HMF yield drastically diminishes from 15.5 to 3.7%. After the second run, a washing with water/acetone and filtration of the used solid was also carried out, recovering the glucose conversion, but the HMF yield is still lower.
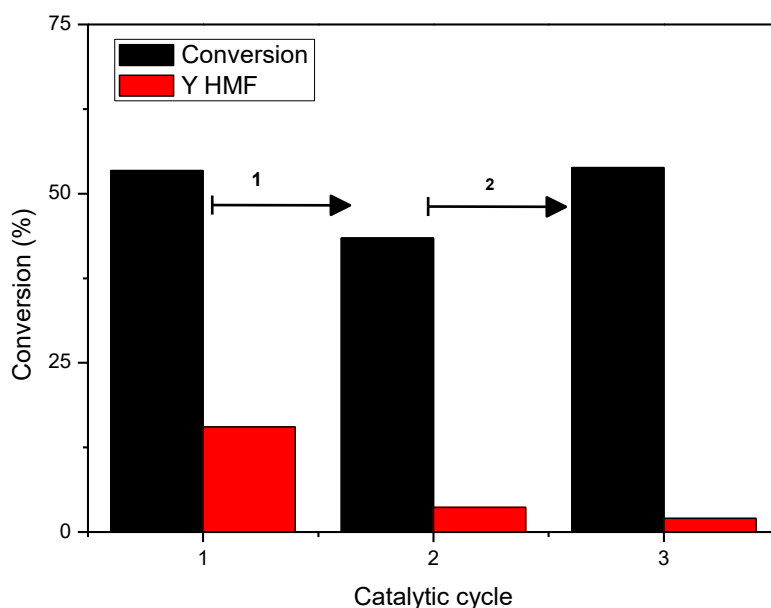
Figure 14. Reusing study of NEEDLE-LTL after (1) drying at 65 ºC and (2) washing with water/acetone (Experimental conditions: 0.15 g glucose, 0.15 g catalyst, 1.5 water, 3.5 mL MIBK, Temperature: 150 ºC; time: 60 min, $CaCl_2$= 0.65 g $g_{H_2O}^{-1}$).

Finally, the used catalyst was calcined until 550 ºC for 2 h after a first catalytic cycle in order to remove the organic fraction. However, the initial catalytic performance continued without recovery, with values of glucose conversion and HMF yield of 100 and 4.52%, respectively. In order to explain the reason of this behavior, the TG-DTA analyses of used and fresh NEEDLE-LTL zeolite were performed. The fresh zeolite shows a weight loss of 10% between room temperature and 200 ºC, associated to the removing of hydration water, without any remarkable weight variation until 900 ºC. However, the used catalyst exhibits a high weight loss in the same temperature range, but with two distinguishable steps, which could be associated to the elimination of hydration water and adsorbed MIBK, account for 20%. Then, a progressive weight loss is observed, but with an important sloop change between 700 and 900 ºC. Thus, a weight loss of 22% is observed between 200 and 900°C, and the high

temperature required to remove organic molecules could be explained by the strong interaction with the catalyst surface inside the micropores. In this sense, a regeneration temperature of 550 ºC was not enough to remove organic species, which cover the active sites responsible of glucose dehydration to HMF. The covering of active sites by carbonaceous deposits, as main cause of the decrease in catalytic activity, has been already reported for zeolites [23].
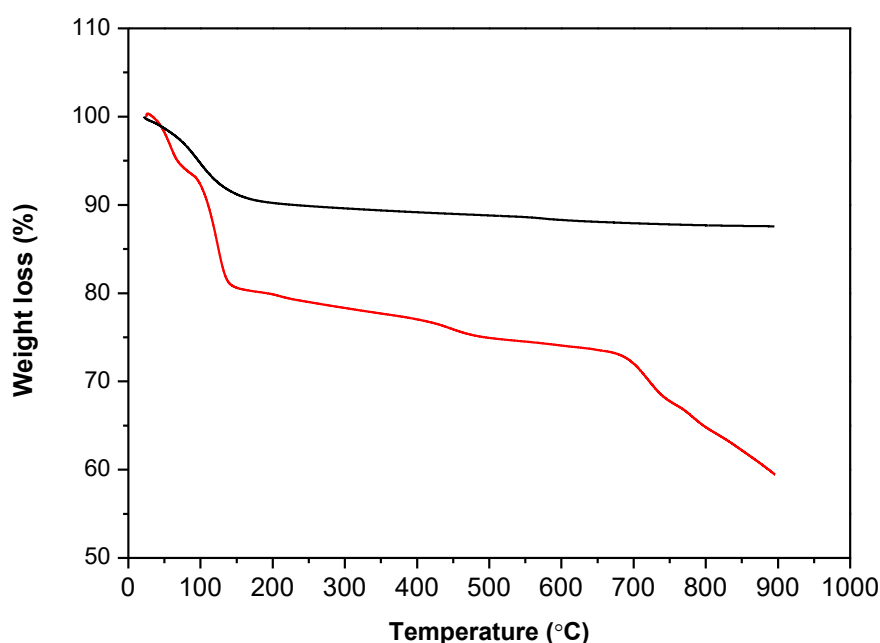
Figure 14. TG-DTA analysis of fresh (black line) and used (red line) (glucose:catalyst weight ratio= 1:1, T= 150 ºC, time= 60 min) NEEDLE-LTL

Therefore, it can be concluded that the diffusion of glucose molecules to active sites present in LTL zeolites is favored by using needle and rod morphologies, but it is necessary to prepare hierarchical zeolites, where mesoporosity is a key feature for facilitating the access of reactants and the regeneration of active sites, and delaying the catalyst deactivation.

3. Experimental

3.1 Chemicals and materials

Potassium hydroxide pellets (85%) and ammonium nitrate were purchased from Merck, Darmstadt, Germany. Colloidal silica HS-40 was supplied by Sigma-Aldrich, Germany. Aluminium sulfate hexadecahydrate ($Al_2(SO_4)_3 \cdot 16H_2O$, 97%) was obtained from BDH Chemical Ltd, Poole, England. All chemicals were used without further purification. For the catalytic tests, the following chemicals have been utilized: glucose (Sigma-Aldrich, >99%), fructose (Sigma-Aldrich, >99%) and calcium chloride (VWR, 97%). Deionized water and methyl isobutyl ketone (MIBK, VWR, 98%) have been used as solvents.

3.2 Synthesis of L-type zeolites

Short-rod shape L-type zeolite was synthesized by dissolving KOH (3.018 g) and $Al_2(SO_4)_3.16H_2O$ (1.442 g) with distilled water (18.208 g) in a polypropylene (PP) bottle. The mixture was magnetically stirred at room temperature to form a slightly cloudy solution. A clear silicate solution was prepared by mixing HS-40 (6.875 g) with distilled water (9.958 g) under stirring for 5 min. To avoid gelation, the silicate solution was added dropwise into the aluminate solution under vigorous stirring for 5 min. The solution with a final molar ratio of 10.0 K_2O : 1 Al_2O_3 : 20 SiO_2 : 800 H_2O was further aged at room temperature for 18 h under stirring prior to crystallization at 180 °C for 3 days. The solid product was then filtered and purified with distilled water until pH 7 prior to freeze-drying. The zeolite powder in K-form (3.000 g) was then ion exchanged with ammonium nitrate (1.5 M, 100 mL) at 25 °C for 18 h before subjecting calcination at 480 °C for 4 h to produce protonated L-type zeolite (ROD-LTL). Similar procedures were used for preparing L-type zeolites with other morphologies (needle and cylinder) but using hydrogels of different molar compositions as stated in **Table 4**. The protonated L-type zeolite crystalline solids with short-rod, cylindrical and needle shapes were denoted as ROD-LTL, CYL-LTL and NEEDLE-LTL, respectively.

Table 4. Experimental conditions for the synthesis of L-type zeolites with different morphologies.

Samples	Molar composition				Aging (h)	Synthesis temperature (ºC)	Synthesis time (h)
	K₂O	Al₂O₃	SiO₂	H₂O			
ROD-LTL	10.0	1	20	800	18	180	72
NEEDLE-LTL	10.2	1	20	1100	18	180	72
CYL-LTL	10.2	1	20	1030	18	180	72

3.3 Characterizations of LTL zeolites

XRD patterns were recorded using a Bruker-AXS D8 diffractometer operating at 40 kV and 10 mA (Cu K$_\alpha$ radiation, λ = 0.15418 nm). The surface morphology of samples was observed using a JEOL JSM-6701F FESEM microscope. The infrared (IR) spectra were acquired using a Perkin-Elmer System 2000 using the KBr method (Sample:KBr ratio = 1:50). The chemical composition of zeolites was also determined with an Optima 8300 inductively coupled plasma-optical emission spectrometer (ICP-OES). Textural properties were determined by a Micrometrics ASAP 2010 nitrogen adsorption analyzer at –196 °C. First, the sample (ca. 0.08 mg) was degassed under vacuum at 300 °C overnight. The surface area and pore size distribution of samples were estimated using the Langmuir and DFT models, respectively. The total pore volume of the solids was determined from the nitrogen adsorbed volume at P/P$_o$ = 0.990.

The FTIR spectra after pyridine adsorption were acquired using a Nicolet 2000 FTIR spectrometer. Initially, the zeolite powder (ca. 0.01 g) was ground and pressed into a self-supporting wafer (area 2 cm^2) at 6.0 ton. The wafer was introduced into an IR vacuum cell and activated at 400 °C for 5 h under vacuum (10^{-3} mbar). The sample was cooled to 25 °C before the background spectrum of zeolite was recorded. Pyridine vapor was adsorbed onto the sample for 3 min before the excess pyridine vapor was evacuated. The FTIR spectra were recorded at 25 °C using 200 scans with a resolution of 6 cm^{-1}. The wafer was then heated at 150 °C for 1

h to remove weakly bound pyridine before the second IR spectrum was recorded. The wafer was heated again to 300 °C for 1 h before it was cooled to 25 °C and scanned again with an IR spectrometer. The concentration of Lewis and Brönsted acid sites were calculated by using the molar integral extinction coefficients of $\varepsilon_{Brönsted} = 3.03$ cm µmol^{-1} and $\varepsilon_{Lewis} = 3.80$ cm µmol^{-1} [reference should be included]

X-ray photoelectron spectra were obtained with a Physical Electronics PHI 5700 spectrometer with non-monochromatic Mg Kα radiation (300 W, 15 kV, and 1253.6 eV) with a multi-channel detector. Spectra were recorded in the constant pass energy mode at 29.35 eV, using a 720 µm diameter analysis area. Charge referencing was measured against adventitious carbon (C 1s at 284.8 eV). A PHI ACCESS ESCA-V6.0 F software package was used for acquisition and data analysis. A Shirley-type background was subtracted from the signals. Recorded spectra were always fitted using Gaussian–Lorentzian curves in order to determine accurately the binding energies of the different element core levels.

^{27}Al MAS NMR experiments were performed on a Bruker AV-400 (9.4 T) spectrometer (Rheinstetten, Germany), using a BL-4 probe with zirconia rotors. The spectra were obtained using a spinning speed of vR = 10 kHz, a pulse width of 1 µs corresponding to a π/12 rad. Pulse length, a relaxation delay of 1 s, and typically 1200 scans. The temperature-programmed desorption of ammonia (NH3-TPD) was carried out to evaluate the total surface acidity of catalysts. After cleaning of catalysts (0.08 g) with helium up to 550 °C and subsequent adsorption of ammonia at 100 °C, the NH$_3$-TPD was performed by raising the temperature from 100 to 550 °C, under a helium flow of 40 mL min-1, with a heating rate of 10 °C min-1 and maintained at 550 °C for 15 min. The evolved ammonia was analyzed by using a TCD detector of a gas chromatograph (Shimadzu GC-14A).

Thermogravimetric analyses (TGA) were performed with a TGA/DSC 1 model (Mettler-Toledo), under air flow of 50 mL min^{-1} with a heating ramp of 10 °C min^{-1}, from room

temperature until 900 ℃. The carbon content of spent catalysts was measured with a LECO CHNS 932 analyser.

3.4 Catalytic reaction

The catalytic performance of LTL-type zeolites in glucose dehydration was evaluated in batch conditions, by using a glass pressure tube with thread bushing (Ace, 15 mL, pressure rated to 10 bars) under magnetic stirring. In a typical experiment, 0.15 g of glucose, 0.05 g of catalyst, 1.5 mL of deionized water and 3.5 mL of methyl isobutyl ketone (MIBK) were introduced into the reactor. Reactors were always purged with nitrogen, prior to the catalytic study, to minimize side reactions of HMF which decrease its yield. The mixture was heated with a thermostatically controlled oil bath. The reaction was quenched by submerging the reactor in a cool water bath, and the liquid phases were separated, filtered and the analysis of products was performed in both phases by high performance liquid chromatography (HPLC). A JASCO instrument equipped with quaternary gradient pump (PU-2089), multiwavelength detector (MD-2015), autosampler (AS-2055), column oven (co-2065) using a Phenomenex Luna C18 reversed-phase column (250 mm × 4.6 mm, 5 µm) and Rezex ROA-Organic Acid H^+ (8%) (300 mm × 7.8 mm, 5 µm), was employed. Both glucose and fructose were monitored using a refractive index detector for aqueous phase, while HMF production was monitored using a UV detector in both phases. The mobile phases consisted in pure methanol (flow rate 0.5 mL·min^{-1}) for Luna C18 and deionized water (flow rate 0.35 mL·min^{-1}) for Rezex ROA, being the columns at room temperature and 40 ℃, respectively.

Conflicts of Interest: The authors declare no conflicts of interest.

References

[1] T. Werpy., G. Petersen., W. T., P. G, **2004**, *1*.

[2] R. Van Putten, J. C. Van Der Waal, E. De Jong, C. B. Rasrendra, H. J. Heeres, J. G. De Vries, *Chem. Rev.* **2013**, *113*, 1499–1597.

[3] D. M. Alonso, J. Q. Bond, J. A. Dumesic, *Green Chem.* **2010**, *12*, 1493–1513.

[4] T. Wang, M. W. Nolte, B. H. Shanks, *Green Chem* **2014**, *16*, 548–572.

[5] I. Delidovich, K. Leonhard, R. Palkovits, *Energy Environ. Sci.* **2014**, *7*, 2803.

[6] A. Corma, S. Iborra, A. Velty, A. Corma Canos, S. Iborra, A. Velty, *Chem. Rev.* **2007**, *107*, 2411–2502.

[7] L. Hu, X. Tang, J. Xu, Z. Wu, L. Lin, S. Liu, *Ind. Eng. Chem. Res.* **2014**, *53*, 3056–3064.

[8] P. Gallezot, *Chem. Soc. Rev.* **2012**, *41*, 1538–58.

[9] D. W. Rackemann, W. O. Doherty, *Biofuels, Bioprod. Biorefining* **2011**, *5*, 198–214.

[10] E. Nikolla, Y. Roman-Leshkov, M. Moliner, M. E. Davis, *Acs Catal.* **2011**, *1*, 408–410.

[11] M. Yabushita, H. Kobayashi, A. Fukuoka, *Appl. Catal. B Environ.* **2014**, *145*, 1–9.

[12] M. J. Climent, A. Corma, S. Iborra, *Green Chem.* **2011**, *13*, 520.

[13] I. Gandarias, P. L. Arias, *Catal. Today* **2014**, *234*, 42–58.

[14] C. García-Sancho, I. Fúnez-Núñez, R. Moreno-Tost, J. Santamaría-González, E. Pérez-Inestrosa, J. L. G. L. G. Fierro, P. Maireles-Torres, *Appl. Catal. B Environ.* **2017**, *206*, 617–625.

[15]   M. Moreno-Recio, J. Santamaría-González, P. Maireles-Torres, *Chem. Eng. J.* **2016**, *303*, 22–30.

[16]   I. Jiménez-Morales, M. Moreno-Recio, J. Santamaría-González, P. Maireles-Torres, A. Jiménez-López, *Appl. Catal. B Environ.* **2015**, *164*, 70–76.

[17]   I. Jiménez-Morales, M. Moreno-Recio, J. Santamaría-González, P. Maireles-Torres, A. Jiménez-López, *Appl. Catal. B Environ.* **2014**, *154–155*, 190–196.

[18]   Y. Yang, C. W. Hu, M. M. Abu-Omar, *Green Chem.* **2012**, *14*, 509–513.

[19]   Y. Román-Leshkov, J. A. Dumesic, *Top. Catal.* **2009**, *52*, 297–303.

[20]   J. Teychené, H. Roux-De Balman, S. Galier, *Carbohydr. Res.* **2017**, *448*, 118–127.

[21]   E. Combs, B. Cinlar, Y. Pagan-Torres, J. A. Dumesic, B. H. Shanks, *Catal. Commun.* **2013**, *30*, 1–4.

[22]   M. Moreno-Recio, I. Jiménez-Morales, P. L. Arias, J. Santamaría-González, P. Maireles-Torres, *ChemistrySelect* **2017**, *2*, 2444–2451.

[23]   S. Xu, D. Pan, F. Hu, Y. Wu, H. Wang, Y. Chen, H. Yuan, L. Gao, G. Xiao, *Fuel Process. Technol.* **2019**, DOI 10.1016/j.fuproc.2019.03.012.

[24]   M. J. Remy, D. Stanica, G. Poncelet, E. J. P. Feijen, P. J. Grobet, J. A. Martens, P. A. Jacobs, *J. Phys. Chem.* **1996**, *100*, 12440–12447.

[25]   J. F. Moulder, W. F. Stickle, P. E. Sobol, K. D. Bombem, *Handbook of X-Ray Photoelectron Spectroscopy*, Perkin-Elmer Corporation, **1992**.

[26]   E. P. Ng, H. Awala, K. H. Tan, F. Adam, R. Retoux, S. Mintova, *Microporous Mesoporous Mater.* **2015**, *204*, 204–209.

[27]   V. P. Valtchev, K. N. Bozhilov, *J. Phys. Chem. B* **2004**, *108*, 15587–15598.

[28]   B. Xu, S. Bordiga, R. Prins, J. A. van Bokhoven, *Appl. Catal. A Gen.* **2007**, *333*, 245–253.

[29]   M. Mu, G. Harvey, R. Prins, **2000**, *34*, 281–290.

[30]   F. R. Chen, J. G. Davis, J. J. Fripiat, *J. Catal.* **1992**, *133*, 263–278.

[31]   A. Galadima, O. Muraza, *Fuel* **2019**, DOI 10.1016/j.fuel.2019.115851.

[32]   D. Prat, A. Wells, J. Hayler, H. Sneddon, C. R. McElroy, S. Abou-Shehada, P. J. Dunn, *Green Chem.* **2015**, *18*, 288–296.

[33]   I. Fúnez-Núñez, C. García-Sancho, J. A. Cecilia, R. Moreno-Tost, E. Pérez-Inestrosa, L. Serrano-Cantador, P. Maireles-Torres, *Appl. Catal. A Gen.* **2019**, *585*, 117188.